



NOVA

University of Newcastle Research Online

nova.newcastle.edu.au

Ruppert, Michael G.; Yong, Yuen K. "Note: Guaranteed collocated multimode control of an atomic force microscope cantilever using on-chip piezoelectric actuation and sensing", Published in Review of Scientific Instruments Vol. 88, Issue 15 August 2017, no. 086109. (2017)

Available from: <http://dx.doi.org/10.1063/1.4990451>

© 2017 AIP. This article may be downloaded for personal use only. Any other use requires prior permission of the author and AIP Publishing.

Accessed from: <http://hdl.handle.net/1959.13/1348658>

Note: Guaranteed Collocated Multi Mode Control of an Atomic Force Microscope Cantilever Using On-Chip Piezoelectric Actuation and Sensing

Michael G. Ruppert^{1, a)} and Yuen K. Yong^{1, b)}

The University of Newcastle, University Drive, Callaghan NSW 2308, Australia

(Dated: 8 August 2017)

The quality (Q) factor is an important parameter of the resonance of the microcantilever as it determines both imaging bandwidth and force sensitivity. The ability to control the Q factor of multiple modes is believed to be of great benefit for atomic force microscopy techniques involving multiple eigenmodes. In this paper, we propose a novel cantilever design employing multiple piezoelectric transducers which are used for separated actuation and sensing leading to guaranteed collocation of the first eight eigenmodes up to 3 MHz. The design minimizes the feedthrough usually observed with these systems by incorporating a guard trace on the cantilever chip. As a result, a multimode Q controller is demonstrated to be able to modify the quality factor of the first two eigenmodes over up to four orders of magnitude without sacrificing robust stability.

Dynamic Atomic Force Microscopy (AFM) operating modes can map the surface topography and material composition of specimen with nanometer spatial resolution by scanning a sharp tip at the end of an actively driven microcantilever over the surface of a sample^{1,2}.

Conventionally, the cantilever is used ‘as is’, i.e. the eigenmodes in terms of their quality (Q) factors are left uncontrolled. However, the Q factor directly affects the imaging bandwidth as the transient response of the i -th mode decays exponentially with the time constant $\tau_i = 2Q_i/\omega_i$ ³. Further, the average tip-sample force \bar{F}_{ts} and the average power dissipation \bar{P}_{ts} are also a function of the Q factor of the active eigenmode^{4,5}.

Originally introduced to reduce the quality factor of the fundamental mode of the cantilever⁶, active Q control can increase the scan speed by reducing the transient response of the cantilever⁷. On the other hand, actively increasing the quality factor was shown to be beneficial for imaging sensitivity⁸, particularly when imaging in liquids⁹.

However, the common method for active modification of the cantilever Q factor is based on the time-delay method¹⁰ which is an easy to implement solution but comes with a number of disadvantages. These include the restriction to controlling the fundamental mode, non-robust stability properties¹¹, and limited damping performance¹². These limitations can be overcome by using model-based resonant controllers although these require integrated actuation to avoid the additional dynamics caused by the stack actuator¹³. With controllers of this type, it was shown that multiple eigenmodes can be controlled simultaneously which enables imaging on higher eigenmodes¹⁴ and optimizing the material contrast in bimodal AFM¹⁵.

The aforementioned Q control methods all rely on feedback from the optical beam deflection sensor, as it remains the most widely used approach to detect

the cantilever oscillations. However, the uncertainty in the position of the laser spot on the cantilever usually leads to a non-collocated actuator-sensor system¹⁴, reducing the stability margins for Q control. This problem can be overcome by integrated sensing methods enabled by microelectromechanical systems (MEMS) fabrication processes such as piezoelectric sensing¹⁶, which were shown to provide multi-mode displacement estimates^{17,18}. The actuator-sensor configuration proposed in this work yields a guaranteed collocated system, a property which is highly desirable for vibration control as it results in guaranteed robust stability of the closed loop¹⁹.

The cantilever geometry chosen for this work is a stepped rectangular design as shown in Fig. 1 which has the benefit of closely spaced higher eigenmodes²⁰. The cantilever consists of a wider section with dimensions of

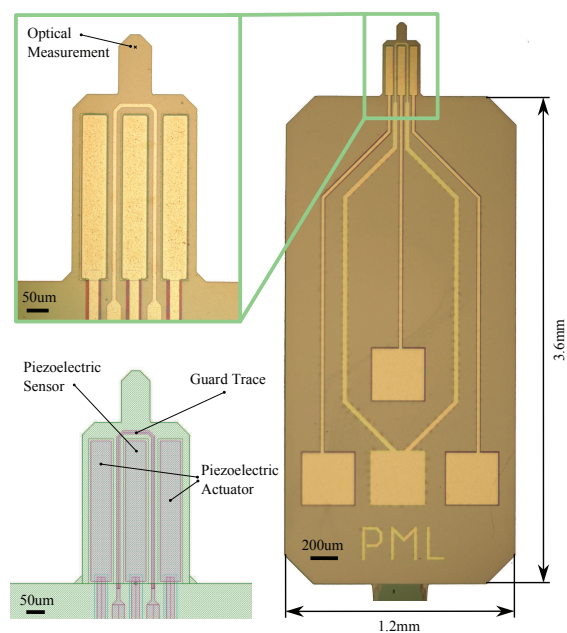


FIG. 1. Design schematic and photo of fabricated piezoelectric MEMS cantilever with integrated actuation and sensing.

^{a)}Electronic mail: Michael.Ruppert@newcastle.edu.au

^{b)}Electronic mail: Yuenkuan.Yong@newcastle.edu.au

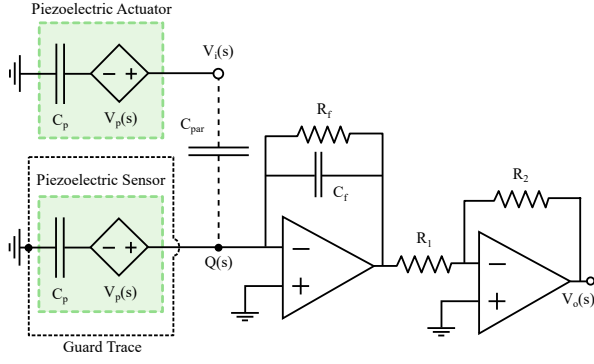


FIG. 2. Implementation of the piezoelectric instrumentation.

$360\mu\text{m} \times 390\mu\text{m}$ and a smaller section with dimensions of $70\mu\text{m} \times 125\mu\text{m}$.

Three laterally symmetric piezoelectric patches are placed on the cantilever, the outer two patches form the actuators and the inner patch serves as the sensor. The equal longitudinal placement of the three transducers guarantees the collocation property of the actuator-sensor system. In order to minimize the feedthrough from the actuators to the sensing patch via the common silicon substrate²¹, a metal guard trace is incorporated which completely surrounds the piezoelectric sensor.

The fabricated design (MEMSCAP, PiezoMUMPs) features a $10\mu\text{m}$ silicon device layer, a $0.5\mu\text{m}$ aluminum nitride piezoelectric layer and chrome / aluminum metal traces²² and is shown in Fig. 1. The schematic of the piezoelectric instrumentation is shown in Fig. 2. The outer piezoelectric patches (drawn as one piezoelectric actuator) are driven by the input voltage $V_i(s)$. A charge-mode amplifier is used as the first stage which amplifies the charge generated by the strain-dependent piezoelectric voltage $V_p(s)$ on the piezoelectric capacitance C_p . The benefit of this circuit is that the high-frequency sensor gain only depends on the feedback capacitance C_f and is independent of the input capacitance at the op-amp. The circuit forms a high-pass filter from piezoelectric charge to first stage output voltage

$$H(s) = \frac{-R_f s}{R_f C_f s + 1}, \quad (1)$$

where the high-frequency charge-to-voltage gain is $1/C_f$ and the corner frequency is given by $f_c = (2\pi R_f C_f)^{-1}$. With the chosen circuit values of $R_f = 1\text{M}\Omega$ and $C_f = 20\text{pF}$, the resulting charge-to-voltage gain is 214 dB and the cut-off frequency is 8 kHz which is adequately lower than the first resonance mode at 62 kHz. An inverting gain stage is added after the charge-mode amplifier for additional gain and accommodating for the negation.

The transfer function from actuator voltage $V_i(s)$ to cantilever deflection $D(s)$ of the first n flexural modes can be described by a sum of second order modes²³

$$G_{dv}(s) = \frac{D(s)}{V_i(s)} = \sum_{i=1}^n \frac{\alpha_i \omega_i^2}{s^2 + \frac{\omega_i}{Q_i} s + \omega_i^2}, \quad \alpha_i \in \mathbb{R} \quad (2)$$

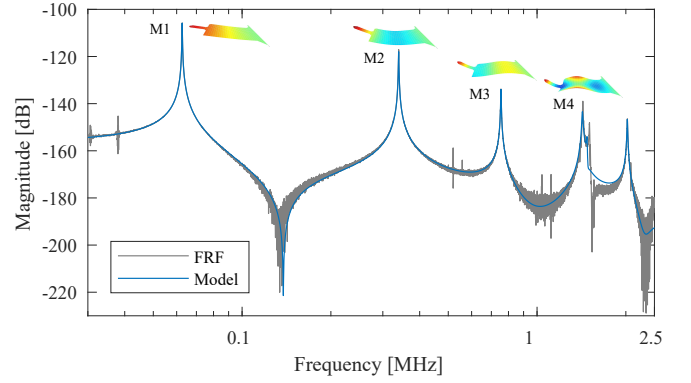


FIG. 3. Frequency response function (FRF) and identified model (2) from actuation voltage to tip displacement (measurement location see Fig. 1) and mode shapes measured with a laser-Doppler vibrometer.

TABLE I. Modal parameters of the first four modes of the cantilever.

	Mode 1	Mode 2	Mode 3	Mode 4
f_i [kHz]	62.6	339.5	754.5	1430.3
Q_i	411	490	320	239
α_i , [nm/V]	12.7	3.41	-0.64	0.48

where each mode is associated with a specific vibrational mode shape, quality factor Q_i , natural frequency ω_i and gain α_i . Note that $\alpha_i \in \mathbb{R}$ does not guarantee that $G_{dv}(s)$ is collocated. Similarly, when a piezoelectric transducer is subjected to mechanical strain, it produces a charge which for the instrumentation chosen here is given by

$$Q(s) = -C_p V_p(s) + D V_i(s) \quad (3)$$

where $D = C_{\text{par}}$ is the parasitic capacitance between actuator and sensor causing a residual amount of feedthrough charge with opposite sign to the motional charge. Within the bandwidth of the read-out circuit, the resulting transfer function from actuator voltage $V_i(s)$ to sensor output $V_o(s)$ is hence described by

$$G(s) = \frac{V_o(s)}{V_i(s)} = -C_p G_{vv}(s) + D \quad (4)$$

where

$$G_{vv}(s) = \frac{V_p(s)}{V_i(s)} = \sum_{i=1}^n \frac{\beta_i \omega_i^2}{s^2 + \frac{\omega_i}{Q_i} s + \omega_i^2}, \quad \beta_i > 0 \quad (5)$$

is the collocated transfer function from actuator voltage to piezoelectric voltage²³. Given that $G_{vv}(s)$ is guaranteed collocated ($\beta_i > 0$), the overall transfer function $-G(s)$ is also collocated for all $D \in \mathbb{R}$.

To control m modes of the cantilever, the positive position feedback controller (PPF)²⁴ of the form

$$K(s) = \sum_{i=1}^m \frac{\gamma_{c,i}}{s^2 + 2\zeta_{c,i}\omega_{c,i}s + \omega_{c,i}^2}, \quad (6)$$

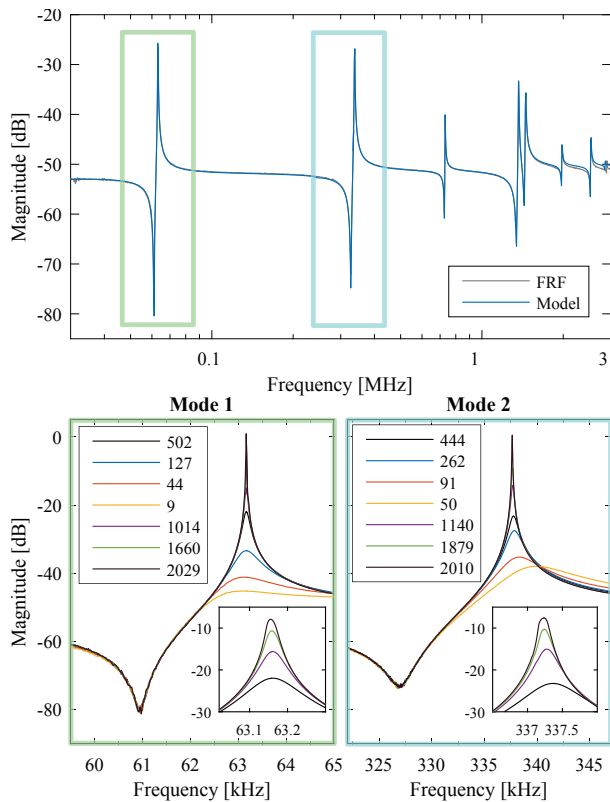


FIG. 4. Top: Open-loop frequency response and model (4) of the piezoelectric sensor. Bottom: Open-loop (black) and closed-loop frequency responses for various controller gains to lower and increase the Q factor of the first and second eigenmode. The achieved Q factors are stated in the legend.

with $\gamma_{c,i}$, $\zeta_{c,i}$ and $\omega_{c,i}$ being the positive tunable controller parameters is used. Controllers of this type used in positive feedback with a collocated system inherit robust closed-loop stability originating from the negative imaginary property of plant and controller if the loop gain is less than one at low frequencies¹⁹.

A laser-Doppler vibrometer (Polytec MSA-100-3D) is used to determine the tip displacement frequency responses and corresponding mode shapes of the cantilever by performing a full modal scan using a periodic chirp excitation signal. The frequency response is shown in Fig. 3 along with the identified model (2) and the mode shapes of the first four flexural modes. From the mode shapes and the pole/zero pattern of the frequency response, it can be clearly observed that the tip displacement is not collocated with the actuation beyond the second mode. The identified parameters of (2) are stated in Table I.

The measured open-loop frequency response of the piezoelectric actuator-sensor system is shown in the top row of Fig. 4 along with the identified model (4). In contrast to Fig. 3, the interlacing poles and zeros are clearly visible up to a frequency of around 3 MHz, showing the collocated characteristic of the proposed design.

Due to its high achievable controller bandwidth of 400 kHz, a field-programmable analog array (FPAA) (Anadigm AN221E04) was chosen for the implementation of the multimode Q controller. The controller was set to adjust the Q factor of the first and second eigenmode by running a pole placement optimization design routine¹⁴. The resulting closed loop formed by $-G(s)$ and $K(s)$ remains stable over a large range of positive parameters values due to the collocated system structure. Therefore, as can be seen from the bottom row in Fig. 4, the Q factors of the first and second mode can be adjusted over a range of four and three orders of magnitude, respectively. On the first mode, an initial Q factor of 502 can be lowered to 9 and increased to over 2000. On the second mode, an initial Q factor of 444 can be lowered to 50 and increased to over 2000. The difference in the dynamic range for controlling the second mode Q factor can be attributed to the controller reaching the bandwidth limitation of 400 kHz.

¹F. J. Giessibl, *Science* **267**, 68 (1995).

²E. T. Herruzo, A. P. Perrino, and R. Garcia, *Nature communications* **5**, 1 (2014).

³T. Ando, T. Uchihashi, and T. Fukuma, *Progress in Surface Science* **83**, 337 (2008).

⁴A. S. Paulo and R. García, *Phys. Rev. B* **64**, 193411 (2001).

⁵B. Anczykowski, B. Gotsmann, H. Fuchs, J. P. Cleveland, and V. Elings, *Appl. Surf. Sci.* **140**, 376 (1999).

⁶J. Mertz, O. Marti, and J. Mlynek, *Appl. Phys. Lett.* **62**, 2344 (1993).

⁷T. Sulchek, R. Hsieh, J. D. Adams, G. G. Yaralioglu, S. C. Minne, and C. F. Quate, *Appl. Phys. Lett.* **76**(11), 1473 (2000).

⁸A. Humphris, A. Round, and M. Miles, *Surface Science* **491**, 468 (2001).

⁹J. Tamayo, A. D. L. Humphris, and M. J. Miles, *Applied Physics Letters* **77**, 582 (2000).

¹⁰T. R. Rodriguez and R. Garcia, *Appl. Phys. Lett.* **82**, 4821 (2003).

¹¹R. W. Stark, in *5th IEEE Conference on Nanotechnology, 2005.* (2005) pp. 259–262 vol. 1.

¹²H. Hölscher, D. Ebeling, and U. D. Schwarz, *J. Appl. Phys.* **99**, 084311 (2006).

¹³M. W. Fairbairn and S. O. R. Moheimani, *Rev. Sci. Instrum.* **83**, 083708 (2012).

¹⁴M. G. Ruppert and S. O. R. Moheimani, *IEEE Trans. Contr. Syst. Technol.* **24**, 1149 (2016).

¹⁵M. G. Ruppert and S. O. R. Moheimani, in *Proc. ASME Int. Design Eng. Tech. Conf. Comput. Inf. Eng. Conf. IDETC/CIE*, Vol. 4 (ASME, Boston, Massachusetts, USA, 2015) p. V004T09A009.

¹⁶T. Itoh and T. Suga, *Nanotechnology* **4**, 218 (1993).

¹⁷M. G. Ruppert and S. O. R. Moheimani, *Beilstein Journal of Nanotechnology* **7**, 284 (2016).

¹⁸S. I. Moore, M. G. Ruppert, and Y. K. Yong, *Beilstein Journal of Nanotechnology* **8**, 358 (2017).

¹⁹I. Petersen and A. Lanzon, *IEEE Control Systems Magazine* **30**, 54 (2010).

²⁰S. Sadewasser, G. Villanueva, and J. A. Plaza, *Rev. Sci. Instrum.* **77**, 073703 (2006).

²¹M. G. Ruppert and S. O. R. Moheimani, *Rev. Sci. Instrum.* **84**, 125006 (2013).

²²A. Cowen, G. Hames, K. Glukh, and B. Hardy, *PiezoMUMPs Design Handbook*, MEMSCAP Inc., 1st ed. (2014).

²³S. O. R. Moheimani and A. J. Fleming, *Piezoelectric Transducers for Vibration Control and Damping* (Springer-Verlag London Limited, 2006).

²⁴J. Fanson and T. K. Caughey, *AIAA Journal* **28**, 717 (1990).